JOURNAL OF GEOPHYSICAL RESEARCH, VOL. 106, NO. D10, PAGES 10,187–10,203, MAY 27, 2001

Atmospheric water vapor over Antarctica derived from Special Sensor Microwave/Temperature 2 data

Jungang Miao, Klaus Kunzi, and Georg Heygster

Institute of Environmental Physics, University of Bremen, Bremen, Germany

Tom A. Lachlan-Cope and John Turner

British Antarctic Survey, Cambridge, England, United Kingdom

Abstract. In polar regions, satellite microwave radiometry has not been successful in measuring the total water vapor (TWV) in the atmosphere. The difficulties faced in these regions arise from the very low water vapor burden of the atmosphere and the large and highly variable emissivities of ice surfaces in the microwave frequency range. By exploiting the advantages of the Special Sensor Microwave/Temperature 2 (SSM/T2), a method is developed to retrieve TWV over Antarctica from satellite data. This method shows very low sensitivities to the change of surface emissivity and to the presence of water clouds. However, ice clouds may have considerable effects. Results of radiative transfer model simulation show that they may cause one to underestimate TWV using the proposed method and that the amount of underestimation is proportional to the ice water path of the ice cloud. Validations using radiosonde measurements and numerical model analyzes suggest that SSM/T2 retrievals have a high accuracy (maximum error $< 10\%$) as long as TWV is $<4.0\,\mathrm{kg\,m^{-2}}$. Above this value, retrievals show a systematic overestimation. Presumably, this is a result of the seasonal difference between the validation and the training radiosonde data sets. TWV retrievals of 1 year's SSM/T2 data show clearly the seasonal variation of water vapor over Antarctica. Throughout the year the mean TWV over West Antarctica is nearly twice as high as that over East Antarctica; the temporal fluctuation of TWV over West Antarctica is also significantly stronger than over East Antarctica. This suggests that precipitation and water vapor transport in West Antarctica are more active than in East Antarctica. Using the same year's TWV data, we estimated the mean residence time of atmospheric water vapor over the Antarctica to be merely 3–4 days. This, however, is much shorter than the global mean of 9–10 days.

1. Introduction

The lack of observations of the atmospheric water vapor content in the Antarctic hinders many studies in this area. For example, research has shown that fluctuations in the mass of the Antarctic ice sheet may significantly impact the variation of global sea level [*Oerlemans*, 1981; *Zwally*, 1989]. As a result, there has been increasing interest recently in the distribution and variability of precipitation over the Antarctic continent [*Bromwich*, 1988, 1990]. However, direct measurement of precipitation is difficult, owing to the strong wind that prevails in a large part of the continent [*Heinemann*, 1997]. At the Antarctic stations, most of which are located in the coastal region, meteorologists have had only little success using snow gauges, since they rapidly fill with blowing snow and it is impossible to distinguish between precipitating and blowing snow [*Turner et al.*, 1997]. The usage of a stake array is a relatively reliable method to measure the snow accumulation, but it is still strongly influenced by blowing snow episodes [*Turner et al.*, 1995] and so does not directly give precipitation. In the interior of the continent there are even fewer direct measurements of precipitation.

Scientists therefore have had to develop alternative methods to estimate the annual precipitation. Two methods have been used. The first one uses glaciological measurements of accumulation. With the help of information about the water mass loss through snow drift across the coastline and liquid water runoff into the ocean, the precipitation is estimated based on accumulation measurements [*Loewe*, 1970; *Bromwich*, 1990]. The second method is to calculate the water vapor transport poleward across the Antarctic coast. The wa-

Paper number 2000JD900811.
0148-0227/01/2000JD900811$09.00

ter vapor is either precipitated as snow or stored as additional water vapor in the atmosphere. The poleward moisture transport has been estimated using outputs of both numerical models [e.g., *Howarth*, 1983; *Giovinetto et al.*, 1997] and radiosonde observations of water vapor and wind profiles from the Antarctic coastal stations [e.g., *Connolley and King*, 1993]. The accuracy of moisture transport estimation is seriously restrained by the insufficient measurement of water vapor in the Antarctic on both temporal and spatial scales. It is also largely restrained by the low reliability of traditional moisture sensors in such a cold environment [*Connolley and King*, 1996]. *Bromwich* [1990] found that there were remarkable disagreements among the estimated annual precipitation over the entire continent derived from the two methods. He suggested that this large discrepancy was a result of deficiencies in evaluating the effects of cyclones and surface winds at the coast when calculating the poleward moisture transport.

Traditionally, upper air humidity measurements at Antarctic stations are made with the help of balloons equipped with one of the two types of humidity sensors: the carbon hygristor and the thin-film capacitive hygristor. However, these sensors perform poorly at low temperature and humidity, leading to large errors in relative humidity measurements. *Connolley and King* [1993] reported an uncertainty of ~20% in total water vapor (TWV) estimated using humidity profiles measured by these sensors. The sensors tend to underestimate the absolute humidity in the Antarctic environment. *Anderson* [1993] pointed out that, owing to a general lack of nucleation sites and the frequent presence of supercooled water fogs in the Antarctic, the near-surface air is often close to saturation or even supersaturated with respect to ice. The humidity sensor, which is usually installed within a porous ice coating, acts as a nucleation site for moisture. As air diffuses through this coating to the surface of the sensor, it becomes saturated with respect to ice at the probe temperature. As a result, the sensor never measures humidity above saturation with respect to ice [*Anderson*, 1994]. In its worst case, the report of these sensors may give a relative humidity as much as a few tens of percent lower than its realistic value, depending on the ambient temperature.

Passive radiometric measurements from satellite have been used for decades for precise measurements of atmospheric water vapor [e.g., *Staelin et al.*, 1976]. In regions like the Antarctic, where measurements of atmospheric parameters are extremely sparse, satellite radiometry potentially provides a valuable source of information, with its good spatial and temporal coverage. However, the unique climatic conditions in the Antarctic, including widespread surface temperature inversions and long-lasting cloud cover, as well as extended periods of darkness, present unique problems for water vapor retrieval using satellite radiometric measurements, especially using those in infrared range. An assessment of the quality of the High-Resolution Infrared Radiation Sounder (HIRS) humidity retrievals, carried out for the Weddell Sea region (Antarctica) by *Köpken and Heinemann* [1995], led to the conclusion that the cloud contamination alone causes 25–45% of HIRS measurements to be rejected by the retrieval scheme. By comparing the retrieved humidity profiles with radiosonde soundings, they noticed that the water vapor signal in the HIRS channels is too weak to adapt the first-guess profile to the reality during the retrieval step. The Special Sensor Microwave/Imager (SSM/I) aboard the Defense Meteorological Satellite Program (DMSP) spacecraft has been very successful in measuring TWV globally [e.g., *Schlüssel and Emery*, 1990]. This success, however, is limited to the ice-free oceans. The problem SSM/I faces in ice-covered polar regions is the very weak water vapor signal together with the large and highly variable signals from ice surfaces.

In November 1991 the DMSP satellite F-11 was launched with a new instrument, the Special Sensor Microwave/Temperature 2 (SSM/T2). It operates with channels near the strong water vapor absorption line centered at 183.31 GHz and is intended to improve the retrieval of water vapor profiles. Although the water vapor signal in SSM/T2 is much stronger than in SSM/I, it is nevertheless difficult to do profiling in polar regions [*Kuo et al.*, 1994; *Wilheit and Hutchison*, 1997]. Since water vapor content in polar atmospheres is extremely low, all SSM/T2 channels see down to the ground surface and the weighting functions at different channels are similar, causing SSM/T2 to be unable to distinguish the water vapor of different levels and only to have sufficient sensitivity to the integrated columnar water vapor. Meanwhile, the ground surface has a significant contribution to all SSM/T2 channels owing to the high transmissivity of the polar atmosphere. In this paper we develop a method to retrieve the TWV using SSM/T2 measurements. This method is capable of dealing with the problems in polar regions and allows the retrieval of TWV without the help of any auxiliary information on the ground surface. Before discussing this method in detail, however, we summarize briefly the characteristics of the SSM/T2 instrument in the next section.

2. Water Vapor Sounder SSM/T2

SSM/T2 is the first operational microwave water vapor sounder to be placed in orbit. It is a scanning, total power microwave radiometer. After its first launch on board the DMSP spacecraft F-11, three more similar instruments have been deployed in orbit aboard F-12 since August 1994, F-14 since April 1997, and F-15 since December 1999, respectively. SSM/T2 has five channels, three near the strong water vapor absorption line at 183.31 GHz and two within the atmospheric windows near 150 and 91.655 GHz. The numbering and locations of SSM/T2 channels in the microwave spectrum are shown schematically in Figure 1 [*Aerojet GenCorp.*, 1990].

SSM/T2 uses a single offset parabolic reflector with

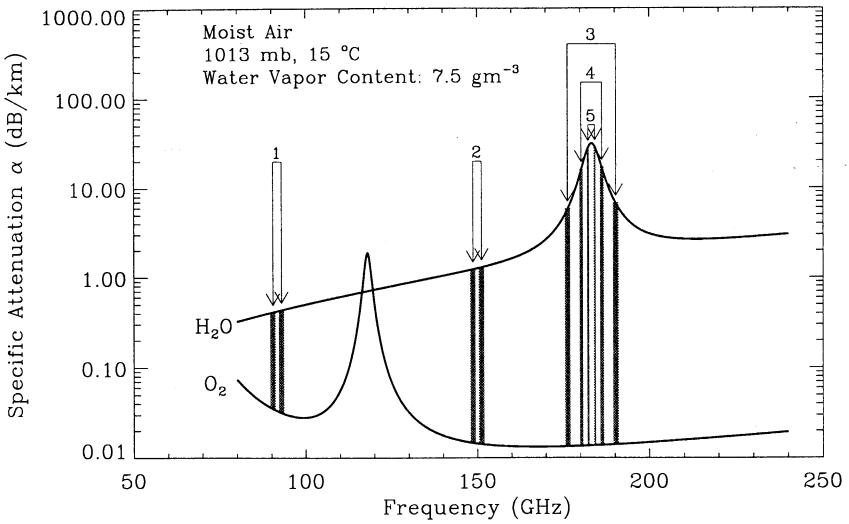

Figure 1. Locations of the five channels of the Special Sensor Micorwave/Temperature 2 (SSM/T2) in the microwave range. The channels are numbered from low to high frequencies, and the shaded stripes indicate the two passbands for each channel. To calculate the specific attenuation of water vapor and oxygen, the International Radio Consultive Committes (CCIR) model given by *Gibbins* [1986] was used.

a projected aperture of 6.6 cm in diameter and a single multifrequency feed horn. This leads to a 3.3° beam width for the 183.31-GHz channels and larger beam widths of ~3.7° and ~6.0° for the 150- and 92-GHz channels, respectively. To perform cross-track scanning, the reflector rotates while the feed horn remains fixed. This results in a rotating polarization state and a changing footprint size. SSM/T2 performs 28 observations (pixels) per scan for each of the five channels, with maximum nadir angle of 40.5°. The 3-dB footprint of the antenna beam projected on the Earth surface for the 183.31-GHz channels are ~48 × 48 km^2 at nadir and ~98 × 66 km^2 at the edge of scan. All five channels have coincident footprint centers. The total swath width for SSM/T2 is ~1500 km. The in-flight calibration is performed by viewing an internal hot-load target (~300 K) and the cosmic background radiation (~3 K) during each scan period. The achieved nominal noise-equivalent delta temperature (NEΔT) is 0.6 K for all channels, except for channel 5, where the nominal NEΔT is 0.8 K. The calibration accuracy of SSM/T2 is 1.5 K.

As a unique feature, all receivers of the SSM/T2 are designed with double sidebands. For the three 183.31-GHz channels the two passbands of each channel are located symmetrically across the center frequency at 183.31 GHz. This feature is very useful. For most terrestrial surfaces the surface emissivity changes smoothly with frequency in the microwave range. Within a narrow band the emissivity-frequency relationship can be assumed to be linear [*Grody*, 1988]. To the first order of approximation, the surface emissivities at the three 183.31-GHz channels are identical. This is the basis of our method to retrieve TWV using SSM/T2 measurements. In the next section we will show that, based on this assumption, the surface signal can be eliminated from SSM/T2 measurements and the water vapor signal is therefore isolated and detected.

Another useful feature of SSM/T2 is its ability to measure the radiance in a mixed polarization state. With Θ representing the satellite scan angle and θ the local zenith angle on the Earth surface, the surface emissivity for SSM/T2, ϵ_s, is given by

$$\epsilon_s = \epsilon_v(\theta)\cos^2(\Theta) + \epsilon_h(\theta)\sin^2(\Theta)\,, \qquad (1)$$

where ϵ_v and ϵ_h denote the vertically and horizontally polarized emissivity of the surface, respectively [*Felde and Pickle*, 1995]. This equation indicates that, when the antenna rotates to view the Earth surface in the nadir, the polarization state of SSM/T2 approaches vertical. (Note that a recent study of *Burns et al.* [1998] shows that the polarization state of SSM/T2 approaches horizontal in the nadir. This, however, does not affect the results of this paper.) Thanks to its mixed polarization state, ϵ_s for SSM/T2 changes with the antenna scan angle to a much less extent than does the emissivity for purely vertical or horizontal polarization. For example, by using the Fresnel formula for specular surfaces and the dielectric constant of seawater given by *Klein and Swift* [1977], the nadir surface emissivity of calm ocean surface at 0 °C is estimated to be ~0.75 at 150 GHz. When the antenna scans from nadir to its outermost position, the emissivities at the vertical and the horizontal polarization change monotonically to 0.88 and 0.52, respectively. However, according to (1), the ϵ_s for SSM/T2 remains close to its nadir value while the antenna scans, with a maximum variation of merely 0.03.

3. Method for Total Water Vapor Retrieval

3.1. Theoretical Basis and Methodology

Our method is based on the radiative transfer theory, which describes the relationship between the radiance observed by a radiometer and the physical properties of the scene observed. In microwave frequency range the radiance is usually represented by an equivalent brightness temperature T_b (in kelvins). For nadir sounding geometry the T_b observed by a spaceborne radiometer is the sum of four contributions: (1) the T_b emitted by the ground surface and attenuated by the atmosphere; (2) the T_b emitted by the atmosphere downward to the ground, scattered by the surface, and attenuated by the atmosphere; (3) the T_b emitted by the atmosphere upward to the instrument; and finally (4) the T_b emitted from the cosmic background, scattered by the surface, and attenuated twice by the atmosphere. Contributions 1, 2, and 4 depend on the properties of both the surface and the atmosphere.

If the atmosphere is free of hydrometeor large enough to induce significant scattering of radiation at a given frequency, the four contributions can be explicitly expressed by the surface and atmospheric parameters. Specular reflection is often used to represent the scattering property for ground surfaces. In this case the T_b observed by a spaceborne radiometer can be written in a simple, contracted form [e.g., *Grody*, 1976]. *Guissard and Sobieski* [1994] have developed a general form of the radiative transfer equation by taking account of the effect of diffuse scattering from the ground surface and the effect of vertical nonuniformity of the atmosphere. Their equation is written as

$$T_b(\theta) = m_p T_s - (T_0 - T_c)(1 - \epsilon_s)e^{-2\tau_0 \sec\theta}, \quad (2)$$

where θ denotes the satellite zenith angle, T_s is the ground surface skin temperature, T_0 is the ground level air temperature (not the 2-m air temperature usually used by meteorologists), T_c is the cosmic background emission ($\sim$3 K), ϵ_s is the surface emissivity, and τ_0 is the total opacity of the atmosphere in the vertical direction. Equation (2) is similar to the equation obtained for an isothermal atmosphere above a specular surface, e.g., the one given by *Grody* [1976]; the only difference is that (2) includes a correction factor m_p. According to *Guissard and Sobieski* [1994], the factor m_p is given by

$$m_p = 1 + (1 - \epsilon_s e^{-\tau_0 \sec\theta})\frac{T_0 - T_s}{T_s} + \frac{S_p - I_p}{T_s}, \quad (3)$$

in which S_p and I_p stand for the corrections concerning the diffuse scattering of the surface and the vertical nonuniformity of the atmosphere, respectively. Since (2) does not contain any approximation, it will give an exact T_b in case all terms in (3) are precisely evaluated.

According to the calculations of *Guissard and Sobieski* [1994] for seawater surfaces, S_p is important only for the horizontal polarization, with a magnitude of a few kelvins. As SSM/T2 operates in a mixed polarization state, S_p is expected to be small and will be neglected in the following discussions. The atmospheric correction I_p is given by

$$I_p = I_1 + (1 - \epsilon_s)I_2 e^{-2\tau_0 \sec\theta}, \quad (4)$$

with I_1 and I_2 having the following forms:

$$I_1 = -\int_0^\infty [1 - e^{-\tau(z,\infty)\sec\theta}]\frac{dT(z)}{dz}dz, \quad (5)$$

$$I_2 = \int_0^\infty [1 - e^{\tau(z,\infty)\sec\theta}]\frac{dT(z)}{dz}dz, \quad (6)$$

respectively. Here $\tau(z_1, z_2)$ is the atmospheric opacity between two levels z_1 and z_2 in the vertical direction and z is the height above the ground surface. The second term on the right-hand side of (4) will be zero when the atmosphere is totally opaque (because $e^{-\tau_0 \sec\theta} = 0$) or fully transparent (because $1 - e^{\tau(z,\infty)\sec\theta} = 0$). It has its maximum for a semitransparent atmosphere. This maximum is of the order of the current radiometer sensitivity (< 1 K) in the case of snow surface (with $\epsilon_s \approx 0.8$ at SSM/T2 frequencies). Therefore this term can also be neglected. The term I_1, in contrast, may be large, depending on the vertical profiles of humidity and temperature in the atmosphere. The calculations of *Guissard and Sobieski* [1994] for a low-latitude atmosphere with a constant temperature lapse rate of 6.5 K km^{-1} show that I_1 can be larger than 10 K if the atmosphere is approaching opaqueness. In polar regions, especially over the Antarctic continent, however, I_1 is expected to be much smaller, because temperature inversions in the lower troposphere prevail: the term $dT(z)/dz$ in (5) changes sign at the top of the inversion layer, causing the contributions to I_1 from below and above top of the inversion layer, to some extent, to cancel each other out. There is another term in the expression of m_p which contains $T_0 - T_s$. This term equals zero, since we can assume temperature continuity across the terrestrial ground surface; that is, $T_0 = T_s$. Summing up, the correction factor m_p depends mainly on I_1 and is close to unity for thin polar atmospheres. Further, if the atmosphere is isothermal, I_1 will be zero and m_p will become unity. In this case, (2) is simplified to

$$T_{0,b}(\theta) = T_s - (T_s - T_c)(1 - \epsilon_s)e^{-2\tau_0 \sec\theta}. \quad (7)$$

In order to show that (7) is an approximate form of (2), we add a zero in the lower index of T_b.

Having two channels with identical surface emissivities, the brightness temperature difference (BTD) measured by the two channels can be written, with the help of (7), as

$$\Delta T_{0,ij} = (T_s - T_c)(1 - \epsilon_s)\left(e^{-2\tau_j \sec\theta} - e^{-2\tau_i \sec\theta}\right), \quad (8)$$

where i and j indicate the channel numbers and τ_i and τ_j are the atmospheric opacities at nadir for the two channels used. Further, if three such channels are available, we can obtain a pair of BTDs. The ratio of the two BTDs is

$$\frac{\Delta T_{0,ij}}{\Delta T_{0,jk}} = \frac{e^{-2\tau_j \sec\theta} - e^{-2\tau_i \sec\theta}}{e^{-2\tau_k \sec\theta} - e^{-2\tau_j \sec\theta}} . \quad (9)$$

Interestingly, the BTD ratio given by (9) is not influenced by surface parameters (T_s and ϵ_s) and is related only to the atmospheric opacities at the three channels (τ_i, τ_j, and τ_k). Here the indices i, j, and k denote the channel numbers.

Under clear-sky conditions the nadir opacity of the atmosphere is determined by the absorptions of gaseous oxygen and water vapor. As a first order of approximation, it can be written as a linear function of the total water vapor W (in $\mathrm{kg\,m^{-2}}$),

$$\tau_x = \kappa_{v,x} W + \tau_{o,x} , \quad (10)$$

where $\kappa_{v,x}$ is the mass absorption coefficient of water vapor and $\tau_{o,x}$ is the partial opacity of oxygen, at the channel x ($= i, j, k$). Since the passbands of SSM/T2 channels are located far away from oxygen absorption lines, oxygen has very little influence on SSM/T2. If any, the influences at the four higher-frequency channels (i.e., the 150-GHz and the three 183.31-GHz channels) are also very close to each other (refer to Figure 1). Consequently, they are canceled out in (9). In order to explicitly relate the BTD ratio to the total water vapor W, we use the transformation introduced by *Miao* [1998]. It transforms the summation of two exponential functions seen in the numerator and the denominator of (9) into the product of a linear and an exponential function

$$e^{-2a_1 x} - e^{-2a_2 x} \approx A_1 x e^{-(A_2 x^2 + A_3 x)} . \quad (11)$$

The coefficients A_1, A_2, and A_3 are simple functions of a_1 and a_2. By using this transformation and (10), (9) changes to the following form:

$$\ln \frac{\Delta T_{0,ij}}{\Delta T_{0,jk}} = c_0 + c_1 (W \sec\theta) + c_2 (W \sec\theta)^2 . \quad (12)$$

The coefficients c_0, c_1, and c_2 only depend on $\kappa_{v,i}$, $\kappa_{v,j}$, and $\kappa_{v,k}$, the water vapor mass absorption coefficients of the used channels.

However, the simple relationship in (12) is obtained by using the approximate expression of T_b, i.e., (7). If the exact expression of T_b in (2) is used, the relationship between the BTD ratio $\Delta T_{ij}/\Delta T_{jk}$ and the total water vapor W will become a little complex. However, it is easy to prove that

$$\Delta T_{ij} = \Delta T_{0,ij} + b_{ij} , \quad (13)$$

$$\Delta T_{jk} = \Delta T_{0,jk} + b_{jk} , \quad (14)$$

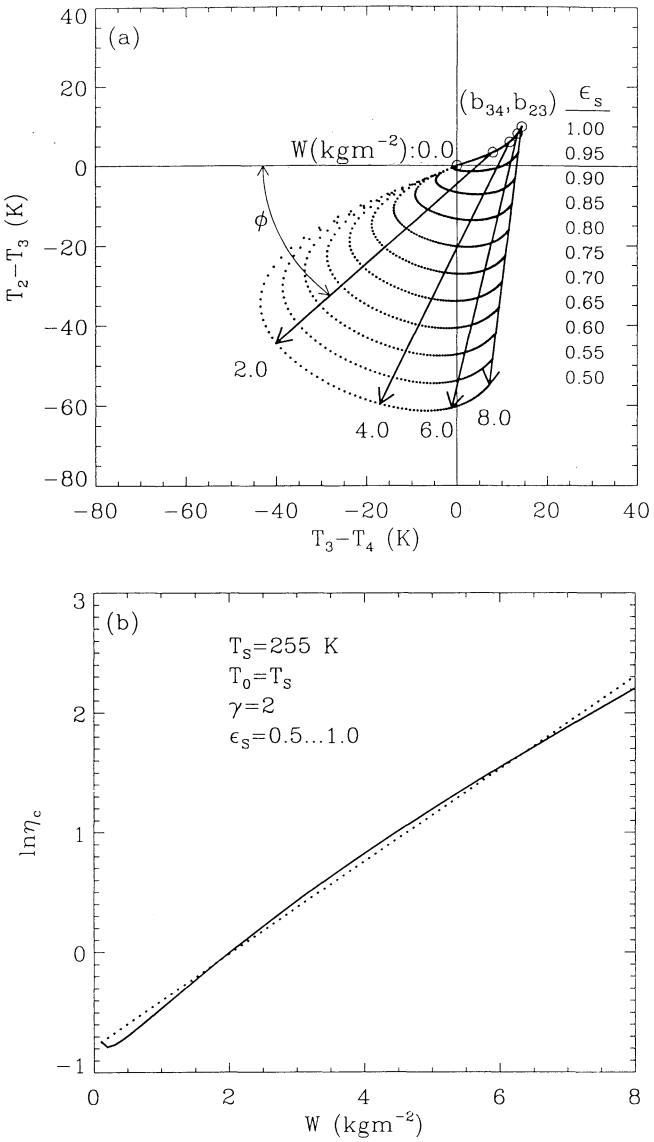

Figure 2. Results of radiative transfer model simulation. (a) The brightness temperature difference (BTD) point ($T_3 - T_4$, $T_2 - T_3$) moves along the dotted lines as total water vapor W increases from 0 to $8\,\mathrm{kg\,m^{-2}}$ in steps of $0.1\,\mathrm{kg\,m^{-2}}$ and along the solid lines as surface emissivity ϵ_s decreases from 1.0 to 0.5 in steps of 0.05. The open circles show positions of the biases (b_{34}, b_{23}). (b) The relationship between $\ln\eta_c$ and W for the simulated brightness temperatures shown in Figure 2a. The dotted line represents the linear part of this relationship.

with b_{ij} and b_{jk} being two quantities (called biases hereafter) that represent the differences caused by using (2) and (7). Combining (2)–(7), one can prove that b_{ij} is given by

$$b_{ij} = \int_0^\infty \left[e^{-\tau_{0,j}(z,\infty)\sec\theta} - e^{-\tau_{0,i}(z,\infty)\sec\theta} \right] \frac{dT(z)}{dz}\, dz . \quad (15)$$

Similarly, the expression of b_{jk} can be obtained by replacing the indices (i, j) with (j, k) in the above equa-

tion. We see immediately that biases b_{ij} and b_{jk} are not influenced by the ground surface; instead, they are only related to the temperature and humidity profiles of the atmosphere. By defining a new quantity,

$$\eta_c = \frac{\Delta T_{ij} - b_{ij}}{\Delta T_{jk} - b_{jk}}, \tag{16}$$

which is called the ratio of the compensated brightness temperature differences (RCBTD), we can maintain the simple form of (12) in relating η_c to W

$$\ln \eta_c = c_0 + c_1(W \sec\theta) + c_2(W \sec\theta)^2 . \tag{17}$$

If we remember that η_c is expressed using the exact BTDs, i.e., ΔT_{ij} and ΔT_{jk}, which are evaluated using the brightness temperatures from (2), we will immediately understand the practical meaning of (17): as soon as the biases b_{ij} and b_{jk} are known, TWV can be retrieved directly from the realistic measurements of SSM/T2.

The theoretical derivation presented in the preceding paragraphs has been verified by numerical simulations using the one-dimensional radiative transfer model, Microwave Model (MWMOD) [*Fuhrhop et al.*, 1998]. Figure 2 gives an example of these simulations carried out for the 2nd, 3rd, and 4th channel of SSM/T2 (refer to Figure 1 for channel number). In the model the surface emissivities at the three channels were always set to same values. The temperature profile in the troposphere was assumed to change linearly with height, decreasing from the surface up to the tropopause at 9 km with a fixed lapse rate of 6.0 $\mathrm{K\,km^{-1}}$. Above the tropopause the temperature was set to be constant. The error induced by this unrealistic temperature distribution is small, since the atmospheric water vapor content above the tropopause is negligible. The specific humidity profile was assumed to be proportional to the γth power of pressure p; γ took values of 1, 2, and 3 in the simulation. The surface pressure p_s was fixed at 1000 mbar. In Figure 2a the simulated brightness temperatures are shown in the plane of $T_2 - T_3$ $(= \Delta T_{23})$ versus $T_3 - T_4$ $(= \Delta T_{34})$. Each point in this plane represents a set of measurements (T_2, T_3, and T_4), which, in turn, correspond to certain values of total water vapor W and surface emissivity ϵ_s. If W is fixed and ϵ_s is allowed to change, point $(T_3 - T_4, T_2 - T_3)$ will move along a straight line. The slope of this line, which equals $\tan\phi$, is found to be proportional to the total water vapor W. According to the geometrical relationship shown in Figure 2a, we get immediately the following identity:

$$\tan\phi \equiv \frac{T_2 - T_3 - b_{23}}{T_3 - T_4 - b_{34}} \equiv \eta_c . \tag{18}$$

From these simulated brightness temperatures we also found that the relationship between $\ln\eta_c$ and W is in a quadratic form as shown in Figure 2b, consistent with (17).

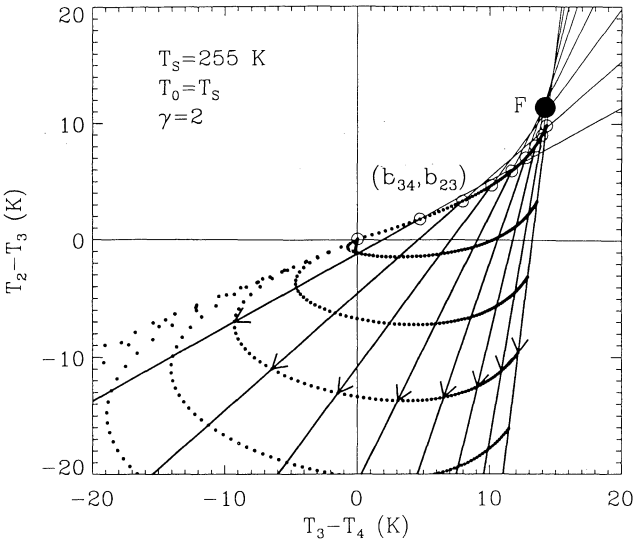

Figure 3. Enlargement of the top right part of Figure 2a. The thin, extended lines intersect each other approximately at the focal point F.

The independence of η_c from surface conditions, together with the simplicity of the relationship between η_c and W, opens a way for us to directly retrieve TWV from SSM/T2 measurements, without having to know the ground surface properties. To do practical retrieval, however, we need to know the biases b_{ij} and b_{jk}. As shown in (15), the biases are functions of the atmospheric temperature and humidity profiles, which are, in most cases, unknown. However, by careful examination of Figure 3, we noticed that all lines, which are with fixed W but changing ϵ_s, intersect approximately at one point, if they are extended in the direction of increasing ϵ_s. This intersection point, denoted by F in the same figure, will be called focal point henceforth. Since η_c is equal to $\tan\phi$, the existence of a focal point F suggests that η_c can be calculated simply using the coordinates of F instead of the real values of b_{ij} and b_{jk}. However, since F is only an approximate focal point, retrievals based on its coordinates will inevitably contain errors. In addition, we found in model simulations that the position of F changes with the atmospheric profiles of temperature and humidity, although to a much smaller extent than do the biases b_{ij} and b_{jk}. In practice, the position of F can be determined with the help of radiative transfer model and radiosonde soundings of the atmosphere collected in regions and time periods of interest. In Table 1 we show the coordinates of F($\bar{b}_{jk}$, $\bar{b}_{ij}$) determined for the Antarctic continent. By using the coordinates of F as the substitutes for b_{ij} and b_{jk} in computing η_c, the surface emissivity is found to influence TWV retrievals, especially when ϵ_s is larger than 0.9. This is simply the result of nonideal compensations of biases b_{ij} and b_{jk} in (16). To improve retrieval accuracy, the algorithm has to be tuned according to the natural range of surface emissivities encountered in re-

Table 1. Focal point F($\bar{b}_{jk}$, $\bar{b}_{ij}$) and coefficients (C_0, C_1) for the Antarctic continent[a]

Channels (i, j, k)	$W \sec\theta$[b] ($\mathrm{kg\,m^{-2}}$)	F($\bar{b}_{jk}, \bar{b}_{ij}$) (K)	C_0, C_1 ($\mathrm{kg\,m^{-2}}$)
3, 4, 5	0.0 – 1.5	2.56, 1.37	0.69, 0.72
2, 3, 4	1.0 – 6.0	4.07, 2.46	2.04, 2.28

[a]These values are determined using radiosonde soundings collected in Antarctic winter at the Antarctic stations Amundsen Scott and Georg von Neumayer.

[b]This is the recommended range of TWV for which the corresponding combination of SSM/T2 channels is suited to do retrieval.

gions of interest. We use a linear algorithm, instead of a quadratic one,

$$W \sec\theta = C_0 + C_1 \ln \eta_c \,, \tag{19}$$

as the quadratic term in (17) is rather small (compare Figure 2b). Here coefficients C_0 and C_1 are constants and they are determined through regression based on model simulations. The values of C_0 and C_1 for the Antarctic continent are given in Table 1.

3.2. Surface Emissivity of the Antarctic Ice Sheet

To tune the TWV algorithm specifically for Antarctica, it is necessary to understand the probable range of surface emissivities of Antarctica at SSM/T2 frequencies. As we know, the Antarctic continent is covered by ice. It is formed through precipitation of snow that has been built up and compressed over thousands of years. Most of the snow cover experiences negligible melting and can be considered dry snow [*Hall and Martinec*, 1985]. So far, there are no in situ measurements reported on the surface emissivity of the Antarctic ice sheet in microwave frequencies. Still, there are some modeling studies using radiative transfer models and observations from satellites [e.g., *Chang et al.*, 1976; *Zwally*, 1977; *Susskind et al.*, 1984]. Using the Electronically Scanned Microwave Radiometer (ESMR) data measured at 19.35 GHz, *Chang et al.* [1976] found emissivities of ~0.7 in the central plateau of East Antarctica and ~0.85 at the base of the Antarctic peninsula. Meanwhile, calculations of *Chang et al.* [1976] showed that the microwave emissivity of dry polar firn depends on the grain or crystal size, which, in turn, depends on the snow accumulation rate. Colder regions tend to have lower accumulation rates and therefore relatively larger grain sizes and lower emissivities than do the warmer regions [*Bindschadler*, 1998]. Accordingly, the coastal regions are generally expected to have higher emissivities than does the continental interior of Antarctica.

In addition to the water vapor sensor SSM/T2, there is another sensor on board the DMSP satellites, which is the Operational Line Scanner (OLS). OLS observes the scene in the visible and thermal infrared bands. By exploiting the concurrent measurements of the microwave and the infrared channels, we have tried to estimate the surface emissivities over the Antarctic continent at the two lower frequencies of SSM/T2. The infrared images from OLS were used to screen out clouds and to determine snow surface temperature in clear-sky situations. SSM/T2 measurements of brightness temperature were directly taken as surface emissions of the ice, as the water vapor emissions are low at 92 and 150 GHz and can be simply omitted. The ratio between the brightness temperatures from SSM/T2 and OLS is then used as an estimate of the surface emissivity. No estimations were done at 183.31 GHz owing to the significant contributions of water vapor for these channels. Data from both SSM/T2 and OLS were available to us for July 25–26, 1995. During these 2 days the Antarctic continent was mostly covered by clouds, especially in the coastal regions. Only part of Queen Maud Land and Wilkes Land on the East Antarctic plateau and parts of West Antarctica, near the Hercules Dome, were recognized as cloud free. Estimations show that, in the 2 days, the surface emissivities in the cloud-free regions were ranging from 0.7 to 0.9 at both 92 and 150 GHz, with the averages close to 0.8. The values at 92 GHz were slightly higher than those at 150 GHz (by ~0.015, on average). It seems that the dry land ice over the East Antarctic plateau has a very week dependence on frequency in its surface emissivity. This conclusion is supported, for instance, for the Queen Maud Land part of East Antarctica, by *Chang et al.* [1976], who reported an emissivity of ~0.75 at 19.35 GHz, and by *Susskind et al.* [1984], who reported an emissivity of ~0.8 at 50.3 GHz. The emissivities given by both *Chang et al.* [1976] and *Susskind et al.* [1984] are evaluated at the horizontal polarization and averaged over the entire scan angles of the respective instrument. For the same region our estimates, which are averaged over SSM/T2 antenna scan angles, are close to 0.8 at both 92 and 150 GHz. A recent study for the coastal regions (around the German Antarctic Station Georg von Neumayer) of the Antarctica was done by *Laue* [1999], who has taken into account the atmospheric water vapor contributions in the SSM/T2 measurements in estimating surface emissivities. His results are that the surface emissivity of the land ice (and shelf ice) near Georg von Neumayer Station lies, in most cases, within the range of 0.7–0.9 at all SSM/T2 frequencies, and the ice surfaces are more emissive in austral winter than in austral summer.

The 150-GHz channel of SSM/T2 will be used later, together with the 183.31-GHz channels, to retrieve TWV, so the difference between the emissivities at these two frequencies is also of concern. According to *Hall and Martinec* [1985], the penetration depth of snow at microwave frequencies is ~10 to 100 times the wavelength, depending upon density, liquid water content, and grain size of the snow. At 150 and 183.31 GHz,

only the top layer (2–20 cm) of the snow is important. Within such a thin layer the temperature of the Antarctic ice sheet can be taken as constant [*Zwally*, 1977]. However, the slightly stronger volume scattering of snow crystals at the higher frequency may cause the surface emissivity at 183.31 GHz to become slightly smaller than that at 150 GHz. Indeed, in examining the SSM/T2 data measured at the 150-GHz channel and the 183.31±7-GHz channel over the dry regions of the Antarctic plateau, we found that the surface emission at 150 GHz is larger than at 183.31 GHz, but by an amount of < 2 K in brightness temperature. Because of the slightly larger surface emission of snow at 150 GHz, an underestimation of TWV may occur when this channel is used for water vapor retrieval. The amount of underestimation depends on both TWV and surface emissivity. For lower emissivities the error is smaller, and it decreases with increasing TWV as the following is true: the larger the water vapor amount is, the less influence the ground surface has. For a typical surface emissivity of 0.8 we found that a 2 K difference in surface emissions at 150 and 183.31 GHz will cause the retrieved TWV to be $\sim 0.2\,\mathrm{kg\,m^{-2}}$ smaller than the real value of $1.5\,\mathrm{kg\,m^{-2}}$. This leads to a relative error of 13%. However, this underestimation reduces to $0.12\,\mathrm{kg\,m^{-2}}$ as the TWV increases to $4.0\,\mathrm{kg\,m^{-2}}$, with a relative error of merely 3%. When TWV is lower than $1.5\,\mathrm{kg\,m^{-2}}$, only the three 183.31-GHz channels are used to do retrieval. In this case, the error induced by ice surfaces is negligibly small, since the ice has nearly identical emissivities for the 183.31-GHz channels.

3.3. Influence of Clouds on Total Water Vapor Retrieval

Clouds influence water vapor retrieval by changing the SSM/T2 brightness temperatures. This happens through absorption and emission from liquid water droplets and through scattering by solid ice crystals within clouds. A thorough understanding of the cloud effect requires quantitative information on both macrophysical parameters (e.g., the base and top height) and microphysical parameters (e.g., water and ice content, particle shape, and size distribution) of the cloud. Compared to the extensive research that has been carried out in the tropics and midlatitudes, there has been very little work on clouds in the Antarctic, especially on in situ measurements of the microphysical parameters [*King and Turner*, 1997]. However, some work has been done using remote sensing instruments. *Stone* [1993] analyzed data from balloon-borne radiometers, which were collected at the South Pole during the austral winter months between 1959 and 1963. These radiometersondes measured vertical profiles of upward and downward longwave radiance of the atmosphere. *Stone* [1993] found that, at the South Pole, cloud bases

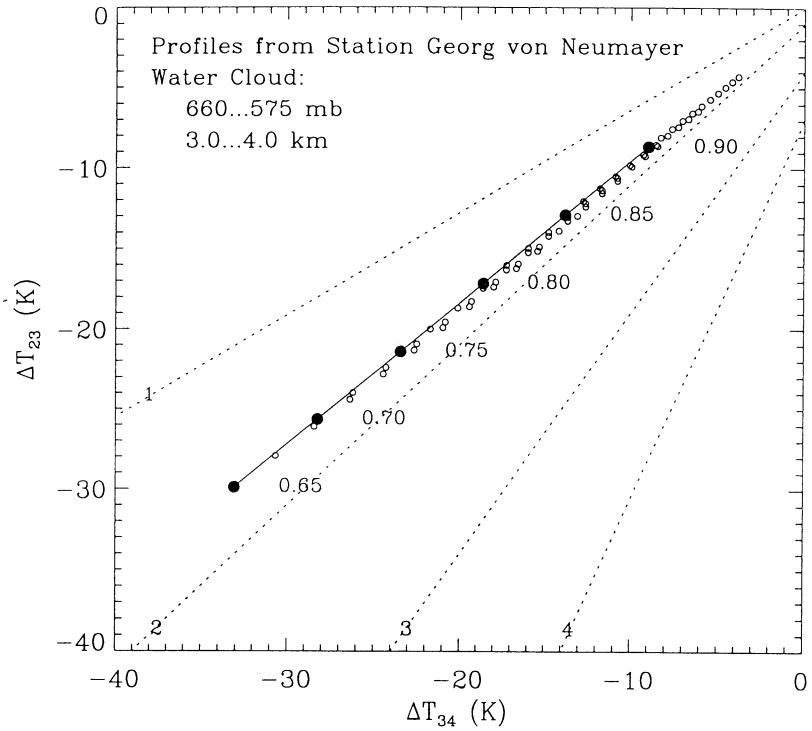

Figure 4. Influence of water clouds on total water vapor retrieval. The large, solid circles indicate the clear-sky situations with ϵ_s changing from 0.65 to 0.9; the small, open circles show cloudy cases. Water clouds cause points $(T_3 - T_4,\ T_2 - T_3)$ to move away from its clear-sky positions toward the origin point (0,0) as the cloud liquid water path grows from zero to $0.3\,\mathrm{kg\,m^{-2}}$. The dashed lines show the contours of constant TWV in $\mathrm{kg\,m^{-2}}$.

generally coincide with the top of the surface-based inversion layer, with an average height of ~465 m. The cloud tops ranged from ~2000 to 6000 m above the surface. Temperatures were as warm as −32 °C in the lowest layers of the clouds and came close to −70 °C at the top of the thickest clouds. Owing to the persistent low temperatures, clouds on the Antarctic plateau are composed primarily of ice crystals. Overall, they are very similar to high-level cirrus clouds observed in midlatitudes. The cloud ice content was estimated to be low, ranging from $\sim 0.3 \times 10^{-3}\,\mathrm{g\,m^{-3}}$ to $6.0 \times 10^{-3}\,\mathrm{g\,m^{-3}}$. Clouds around Antarctica's coast are relatively warm and may contain significant concentrations of liquid water droplets. One year's lidar observations at the French station Dumont d'Urville (66.7 °S, 140 °E) revealed prevailing stratiform low clouds with a midcloud temperature of ~−20 °C in many cases [*del Guasta et al.*, 1993]. These low clouds are believed to be associated with the inversion layer at 1000–3000 m, which prevails in most of the months. The tropopause height varied between 8 and 9 km throughout the year, and cirrus clouds were found to extend up to this level.

To examine cloud effects on TWV retrieval using SSM/T2 measurements, the one-dimensional radiative transfer model MWMOD was used again to do simulations. Atmospheric temperature and humidity profiles collected at the Antarctic Amundsen Scott and Georg von Neumayer stations were used to represent the atmospheres of the continental interior and the Antarctic coast, respectively. In doing model simulations, clouds were taken as vertically homogeneous and the hydrometeors were regarded as spherical. The size distribution model given by *Ulaby et al.* [1981] for midlatitude cirrostratus was used for the Antarctic ice clouds. The stratus model of *Ulaby et al.* [1981] and the altostratus model of *Chylek and Ramaswamy* [1982] were used, respectively, for the low- and middle-altitude water clouds near the Antarctic coast. Simulations show that clouds at different levels have different effects. Generally, low clouds have much smaller influence than medium and high clouds. In particular, water clouds are found to have only negligible influence. This can be explained by the nearly identical absorption rates of water droplets at the SSM/T2 channels used (i.e., the 150- and 183.31-GHz channels). An example for water clouds using the 2nd, 3rd, and 4th channels of SSM/T2 is shown in Figure 4. Since water droplets absorb strongly at high frequencies, the BTDs (ΔT_{23} and ΔT_{34}) decrease dramatically with the increase of cloud liquid water path. However, the BTD points (ΔT_{23}, ΔT_{34}) in cloudy cases lie always close to the line of cloud-free W. Because of the slightly smaller cloud liquid water absorption rate at 150 GHz (the 2nd channel of SSM/T2), TWV retrieved in the case of water cloud is slightly larger than its true value. Ice clouds, in contrast, were found to have much greater influences. Clouds located in medium altitudes have larger effects than do those on high levels. This

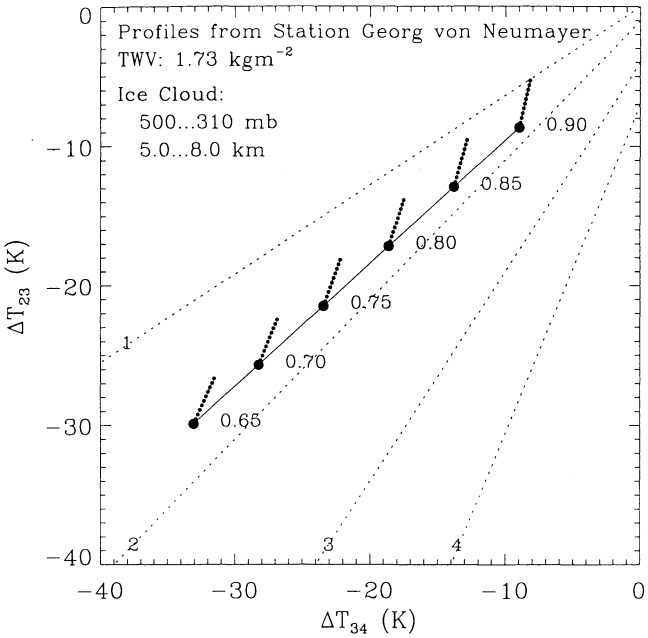

Figure 5. Influence of ice clouds on total water vapor retrieval. The large, solid circles represent the clear-sky situations with ϵ_s changing from 0.65 to 0.9; the small, solid circles show cloudy cases. Ice clouds cause the measurements ($T_3 - T_4$, $T_2 - T_3$) to move away from its clear-sky positions as the cloud ice water path grows from 0 to $60\,\mathrm{g\,m^{-2}}$ with a step of $6\,\mathrm{g\,m^{-2}}$. The dashed lines represent the contours of constant TWV in $\mathrm{kg\,m^{-2}}$.

phenomenon can be explained by the fact that the total water vapor amount above cloud top usually decreases with cloud top height and higher clouds tend to have more similar effects on the brightness temperature measurements at SSM/T2 channels. Therefore, higher clouds have weaker effects on BTDs and then on η_c. Generally, the presence of ice clouds will cause an underestimation of TWV. The amount of underestimation increases with increasing surface emissivity and cloud ice water path, but it decreases with increasing TWV. To give an idea of ice cloud effects, an example is shown in Figure 5. For a typical case of surface emissivity (0.8) and TWV ($1.73\,\mathrm{kg\,m^{-2}}$) we estimated the retrieval error to be as large as 21% when the cloud ice water path was $60\,\mathrm{g\,m^{-2}}$. Nevertheless, the problem of ice clouds is expected to be not very serious, because clouds over the continent have very low ice contents [*Stone*, 1993]. In the coastal regions, they may contain a significant amount of ice, but at the same time, the TWV of the atmosphere is high.

3.4. Validation

The RCBTD method proposed in this paper has been validated through a series of comparisons carried out using TWV data from other independent sources, e.g., radiosonde soundings and numerical model analyzes.

In the first step retrievals of total water vapor using SSM/T2 brightness temperatures simulated with the help of MWMOD were compared with the TWV values derived directly from radiosonde soundings. For this study the radiosonde data available contain three groups of soundings, all of which were obtained in the austral winter. The first group consists of soundings made in June and July of 1992 when the research vessel R/V Polarstern was crossing the Weddell Sea during the Winter Weddell Gyre Study (WWGS). During the 2 months, radiosondes were launched 4 times a day, producing a total of 156 soundings. The second group is composed of 294 soundings launched in June and July 1990–1994, at the German station Georg von Neumayer (70.7 °S, 8.4 °W, 42 m above sea level). The soundings in the third group were made in 1993 using National Oceanic and Atmospheric Administration (NOAA) ozonesondes at the Amundsen Scott station on South Pole (90 °S). As there were initially only nine soundings within June and July in the third group, the soundings of March to May and September to October were included. This expanded the sounding number of the third group to 52. For the purpose of validation, the radiosonde data were then divided into two sets: the training and test set. Each set has 251 soundings with equal numbers of soundings from the aforementioned three groups. The training set was used to optimize the TWV retrieval algorithm, i.e., to determine the coordinates of the focal point F (mentioned in section 3.1) and the coefficients C_0 and C_1 in (19). The test set was used to make a comparison. Its result is shown in Figure 6. For clarity, only retrievals at the minimum and maximum antenna scan angles (corresponding to the minimum and maximum local zenith angles of 1.7° and 47.26°, respectively) are shown. For each radiosonde sounding, seven retrievals were done as the surface emissivity was changing from 0.68 to 0.92 with a step of 0.04. Clearly, the TWV retrieval shows good quality. Especially, when TWV is lower than 4.0 kg m^{-2}, the maximum of relative errors is <10%. For higher TWV the retrieval error can be >10%. In general, error increases as TWV and ϵ_s increase. This is simply caused by the nonideal compensation of biases b_{ij} and b_{jk} when we use the coordinates of the focal point F as their substitutes. Overall, TWV retrievals using simulated brightness temperatures of SSM/T2 compare favorably with the radiosonde measurements of TWV in the range of 0–6.0 kg m^{-2}.

The second comparison was made using real SSM/T2 data from satellite and analyzes of the European Centre for Medium-Range Weather Forecasts (ECMWF) model. As only a limited amount of ECMWF data was available, the comparison was performed for December 1997. The TWV retrievals from SSM/T2 data were mapped onto a grid, which covers the entire Antarctic continent. Each day, we obtained a TWV map over Antarctica, which was a mosaic of the TWV retrievals done for the 14 overflights of satellite within the day. The TWV map from the ECMWF model was an average of the four synoptic analyzes for 0000, 0600, 1200, and 1800 UTC of the day. The spatial resolution of SSM/T2 is, on average, ~70 km, and the one of ECMWF is 1.125° in latitude and longitude. For convenience, comparisons were carried out directly at each grid point (with a spatial resolution of 10 km). Figure 7

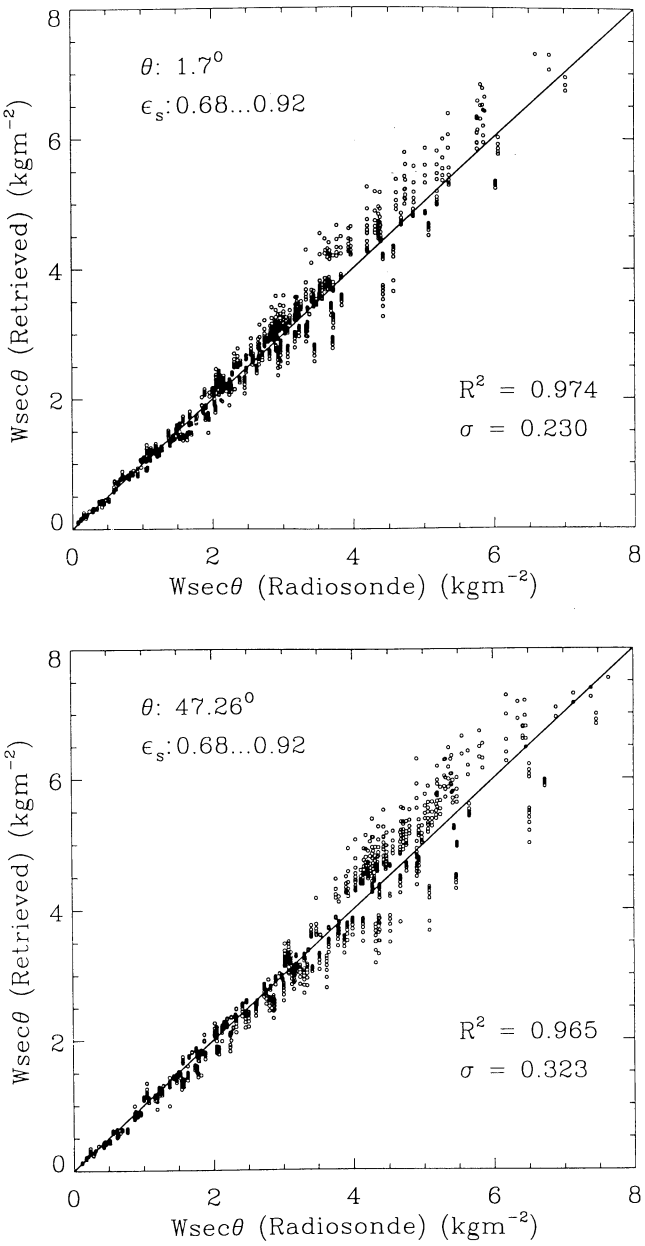

Figure 6. Comparison of the TWV retrieved using simulated brightness temperatures of SSM/T2 and derived from radiosondes. For each radiosonde sounding we have seven TWV retrievals from SSM/T2, which correspond to the seven surface emissivities between 0.68 and 0.92 with an interval of 0.04. (Top) Comparison as the satellite zenith angle is at its minimum of 1.7°. (Bottom) Comparison as the satellite zenith angle is at its maximum of 47.26°. R is the correlation coefficient; σ is the standard deviation.

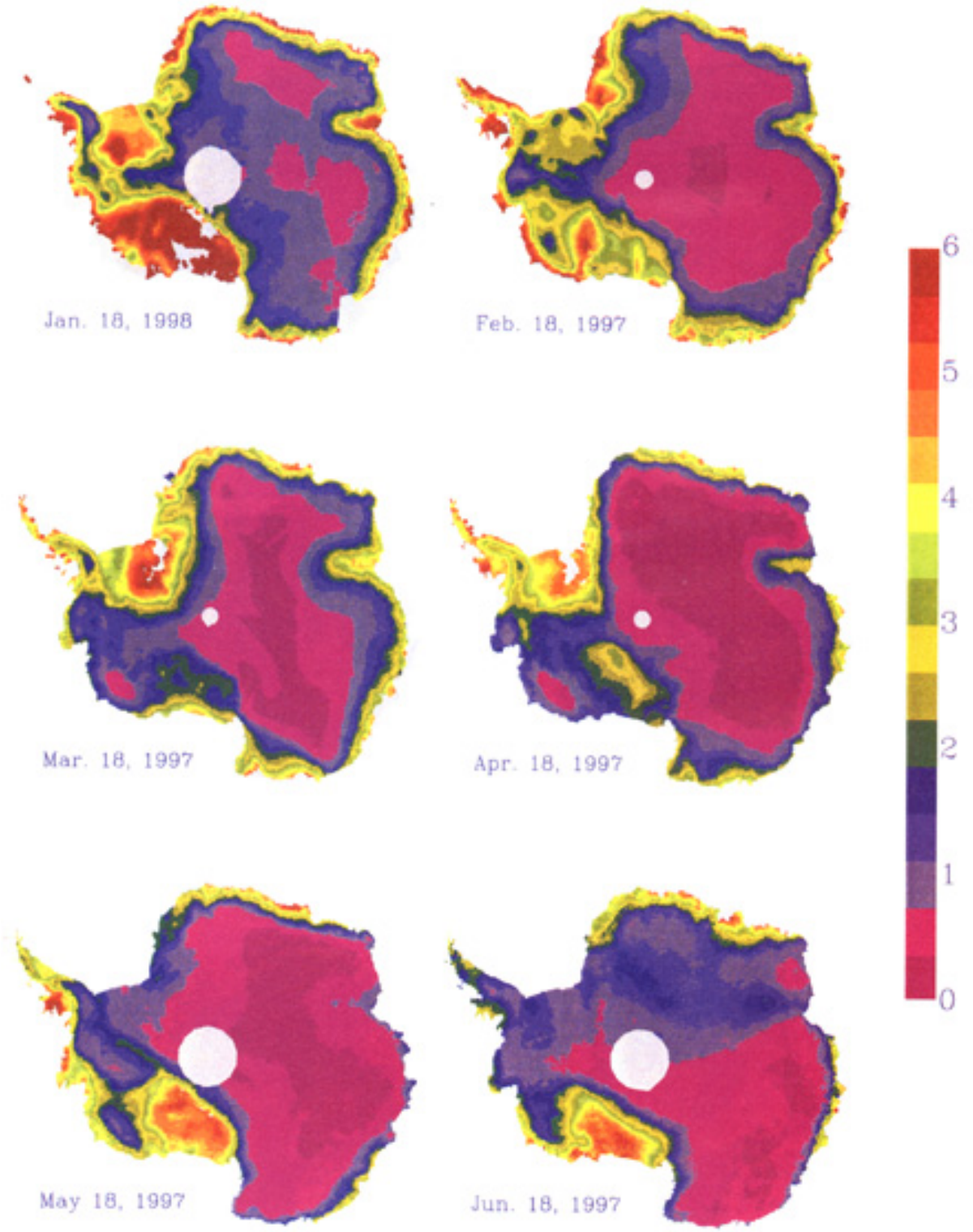

Plate 1. Daily-averaged total water vapor (TWV) (in units of $\mathrm{kg\,m^{-2}}$) maps over Antarctica in a year's circle, from February 1997 to January 1998. The light grey areas in coastal regions indicate cases of missing data or with TWV being so high (i.e., $W \sec\theta$ is $>6.0\,\mathrm{kg\,m^{-2}}$) that the two most sensitive channels of SSM/T2 are already saturated. Maps with large (small) polar holes are derived using SSM/T2 data from DMSP satellite F-14 (F-12).

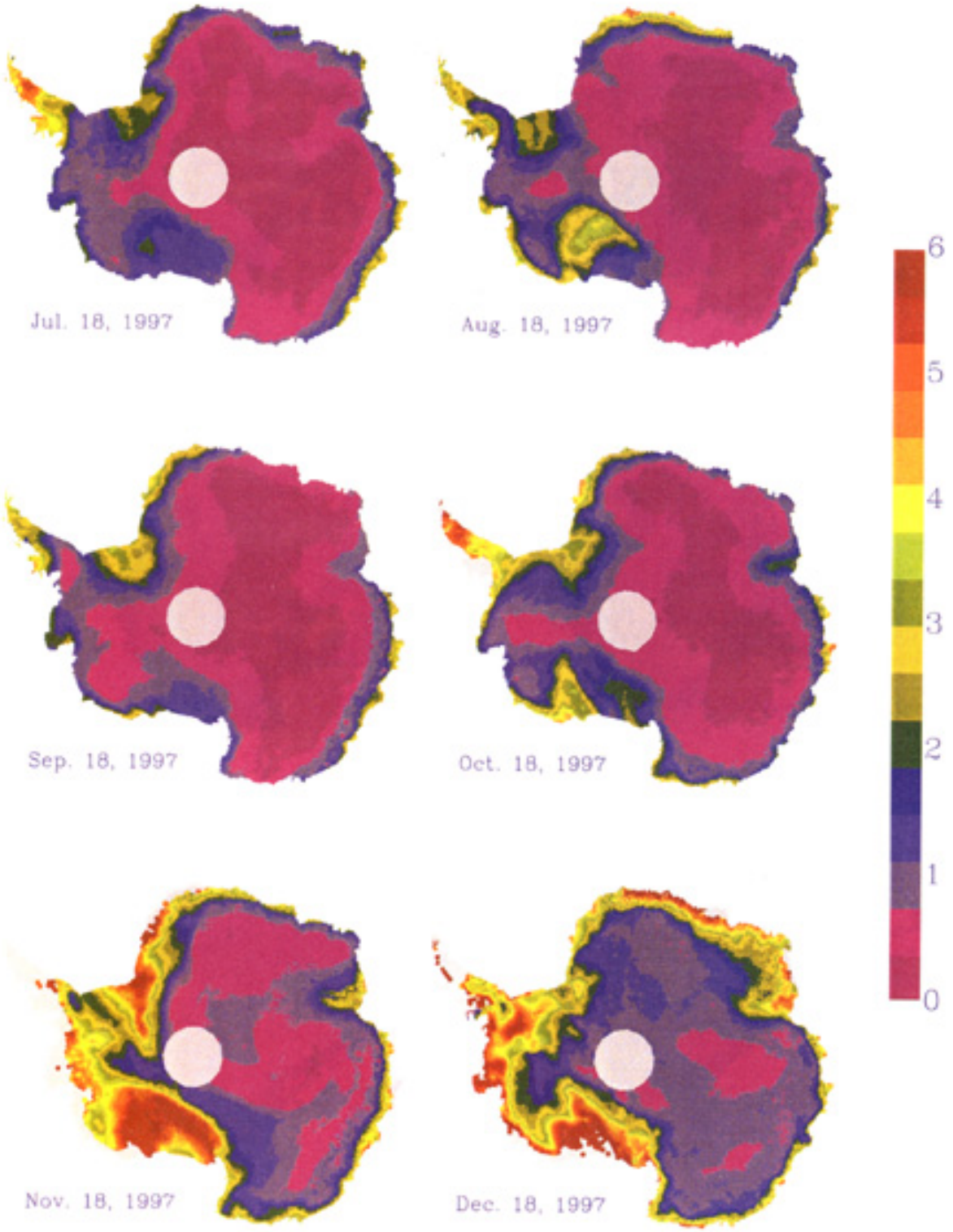

Plate 1. (continued)

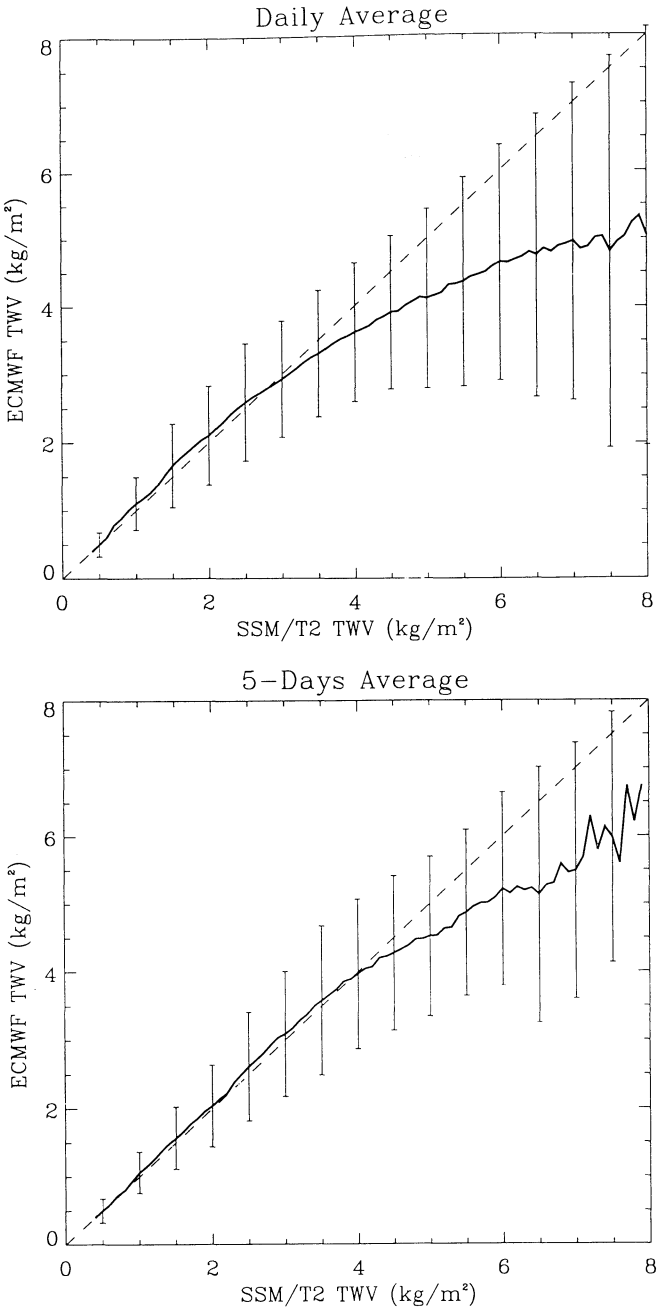

Figure 7. Comparison of the TWV retrieved using real SSM/T2 data and delivered by the European Centre for Medium-Range Weather Forecasts (ECMWF) analyses. Solid lines represent the average TWV over (top) 1 day and (bottom) 5 days. The error bars correspond to 1 standard deviation. This comparison was made for data in December 1997.

shows the results for both daily and 5-days averages. Similar to the preceding comparison using radiosondes, there is good agreement between SSM/T2 retrievals and ECMWF analyzes for TWV lower than $\sim 4.0\,\mathrm{kg\,m^{-2}}$. For higher TWV values, SSM/T2 retrievals present a systematic overestimation. A similar phenomenon was also observed in comparing SSM/T2 retrievals in the same month with coincident radiosonde soundings done at the Halley Station (75.5 °S, 26.4 °W, 32 m above sea level). In December 1997, 30 radiosonde soundings were collected at this station and half of them had to be rejected because of suspicious recordings. Only nine of the qualified soundings had SSM/T2 measurements that lay within the $50 \times 50\,\mathrm{km^2}$ square surrounding the Halley and had a time difference <3 hours in measurements. The overestimation observed in SSM/T2 retrievals is most likely caused by the SSM/T2 algorithm, which was originally tuned using radiosonde soundings for austral winter. However, the frequent failure of the ECMWF model and radiosondes (only one release each day in December 1997) to catch mesocyclones in Antarctic coastal regions may also contribute to this overestimation, because mesocyclones are usually associated with a large amount of water vapor transport.

4. Water Vapor Distribution over Antarctica: Preliminary Results from SSM/T2

4.1. Climatological Study

The DMSP satellites are in a circular, Sun-synchronous, near-polar orbit at an altitude of ~830 km, with an inclination of 98.9° and an orbit period of 101.6 min [*Kramer*, 1996]. Each satellite produces 14.1 full orbits a day. With its 1500-km swath width, SSM/T2 has nearly 100% coverage in polar regions within 1 day. This enables us to obtain daily averaged TWV maps over Antarctica from the satellite data of SSM/T2; and therefore long-term feature of the Antarctic water vapor distribution can be analyzed on the basis of measured water vapor data. However, there are some problems with SSM/T2 satellite data. At first, the data became available relatively late (after 1994) to the research community, although the first SSM/T2 instrument had already been in orbit since 1991. Besides, the 150-GHz channel of the first SSM/T2 on board F-11 failed in the summer of 1993. Moreover, the measurements at the three leftmost scan positions (pixel numbers 26–28) of this instrument were found to be seriously interfered by the glare obstructor, which was designed to keep sunlight out of the instrument cavity [*Kleespies*, 1996]. In processing data from the SSM/T2 on board F-14, we noticed similar problems in the three leftmost scan positions. To avoid suspicious results, measurements of F-14 SSM/T2 at these three positions were not used for TWV retrieval.

With the help of SSM/T2 data, mainly from the year of 1997, climatological analyzes were made and some interesting features of the Antarctic water vapor distribution were observed. Plate 1 shows examples of daily-averaged TWV imagery over Antarctica for a year's circle (from February 1997 to January 1998). Although only one image is shown for each month, the seasonal variation of Antarctic water vapor can be clearly perceived. In the short austral summer, from December to January, there is significantly more water vapor in the atmosphere than during other seasons. This is certainly

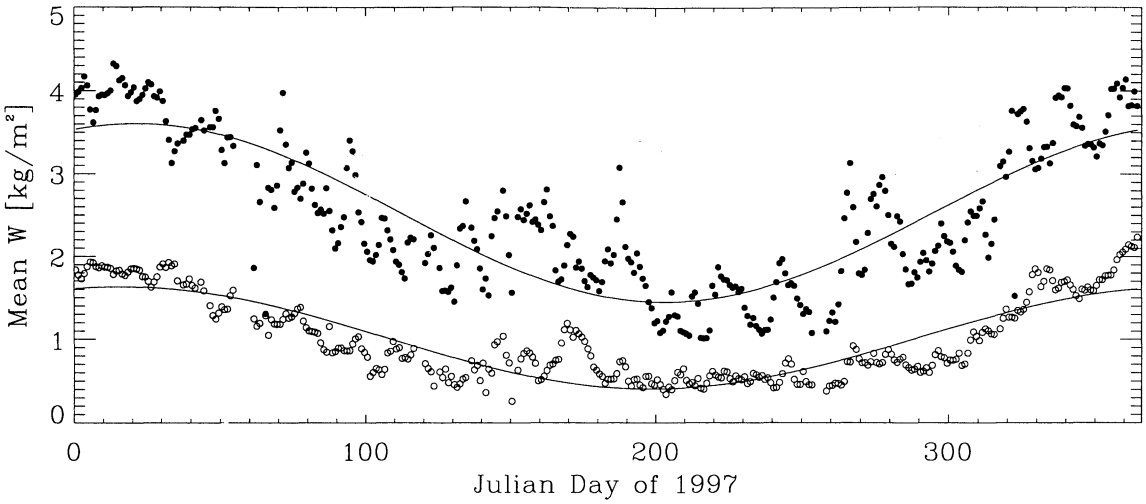

Figure 8. Mean TWV (averaged over 1 day) over East Antarctica (open circles) and West Antarctica (full circles), retrieved from satellite data of SSM/T2 for the year of 1997. The solid lines show the least squares sine waves fitted to 1 year's data.

related to the high air temperatures in summer. Over the elevated plateau of East Antarctica the water vapor content is much lower than over the coastal regions and ice shelves. The Antarctic peninsula is recognized as one of the regions in Antarctica with a large water vapor burden throughout the year, obviously the result of the relatively warm and moist circumpolar westerlies.

In Figure 8 the mean TWV over East and West Antarctica is shown for all of 1997. For the convenience of calculation, East and West Antarctica are simply separated by the meridional lines at 0° and 180° longitude. This picture shows a clear annual oscillation in TWV, with the minimum in both East and in West Antarctica occurring during the austral winter. The pattern shown here is similar to the one given by *Connolley and King* [1993] for the Antarctic station Molodezhnaja. The atmospheric water vapor content in both East and West Antarctica starts to decrease at about the end of January (Julian day 30), as the austral summer begins to lapse. This trend continues until about the end of April (Julian day 120). In East Antarctica there is no significant trend between the end of April (Julian day 120) until mid-November (Julian day 310). The pattern seen in East Antarctica during winter months is similar to the "coreless" winter pattern seen in the winter surface temperature. Such a pattern in East Antarctica is probably a result of the air mass over East Antarctica becoming isolated. (However, wintertime blocking may severely disturb the normal condition in the continental interior and induce strong poleward transport of heat and moisture. *Hirasawa et al.* [2000] observed remarkable increases in temperature and humidity throughout

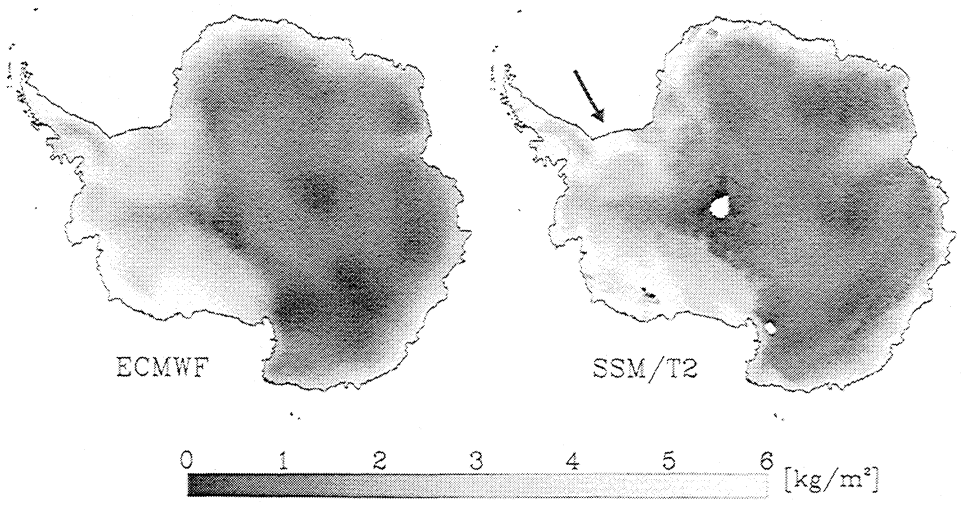

Figure 9. Daily-averaged TWV imagery on December 20, 1997, derived from (left) ECMWF analyses and (right) SSM/T2 measurements. The cyclone over the Ronne Ice Shelf, indicated by the arrow, can be identified in the SSM/T2-derived TWV imagery by the hooklike region with high TWV values.

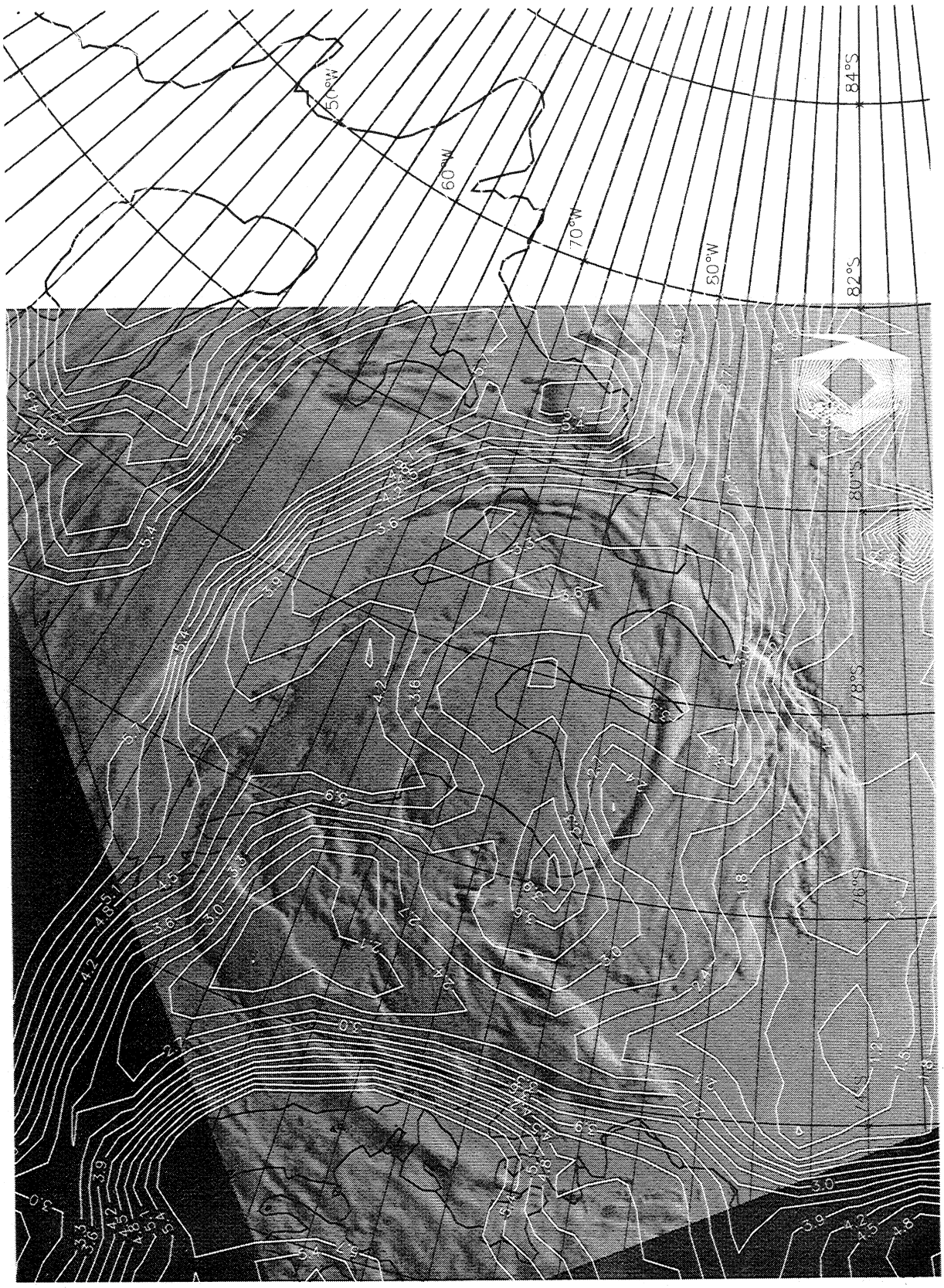

Figure 10. Visible imagery from the Advanced Very High Resolution Radiometer (AVHRR) for the region surrounding the Ronne Ice Shelf at 0124 UTC on December 21, 1997, overlaid with TWV retrievals from SSM/T2 at 0200 UTC on the same day. The thick, black lines indicate coastline and edge of ice shelf; the white lines show TWV contours in units of kg m^{-2}.

the troposphere at the Dome Fuji Station (77 °S, 40 °W, >3800 m above sea level) during June 17–18 (Julian day 168–169), 1997, when a prominent wintertime blocking event developed over East Antarctica. From the TWV image for June 18, 1997, in Plate 1 and the mean TWV values around Julian day 169 in Figure 8, we can clearly see the abrupt increase in TWV over the East Antarctica.) The TWV over West Antarctica shows a distinct minimum just after midwinter (Julian day 200), and, in this case, the pattern is similar to that found in the air temperature at coastal stations. It is not surprising that the pattern of total water vapor follows the temperature so closely. Partially owing to the lower surface elevation, TWV over West Antarctica is higher, almost twice as large as that over East Antarctica throughout the year. Moreover, the temporal fluctuation of the mean TWV is stronger over West Antarctica than over East Antarctica. This indicates that precipitation and water vapor transport are more active in West than in East Antarctica. Meanwhile, the total amount of atmospheric water vapor (integrated within the whole volume above the ground surface) over West Antarctica is larger than that over East Antarctica throughout most of the year, despite the fact that West Antarctica comprises only 35% of the total area of the entire Antarctic continent. The annual mean of the total amount of atmospheric water vapor over the entire continent is estimated to be $\sim 20 \times 10^{12}$ kg. According to *Jacobs et al.* [1992], the total accumulation through snow falling over the Antarctic ice sheet is $\sim 2000 \times 10^{12}\,\mathrm{kg\,yr^{-1}}$. This implies that the mean residence time of water vapor over Antarctica is only 3–4 days, which is significantly shorter than the global mean of 9–10 days [*Howarth*, 1983].

4.2. Case Study

Just as the study of long-term climatological variation of TWV, the method outlined in this paper can be used for case studies of individual events. During December 20, 1997, a mesocyclone developed on the low-lying Ronne ice shelf. Since there are very few in situ measurements made on the Ronne Ice Shelf and no upper air data, the ECMWF analysis for this point of time does not resolve this feature (compare Figure 9), although the area is within a weak trough of low pressure extending from the Weddell Sea over the ice shelf toward the pole. The NOAA Advanced Very High Resolution Radiometer (AVHRR) image for 0125 UTC on December 21 (compare Figure 10) shows the mesocyclone having a distinct spiral form with its center at 78 °S, 83 °W. A clear slot can be seen in the cloud between 60 °W and 65 °W, extending onto the Ronne Ice Shelf from the Weddell Sea. To the east of the clear slot, a broad band of cloud can be seen spiraling into the mesocyclone. Although the satellite imagery can tell us much about the general size and structure of the mesocyclone, the total water vapor retrievals tell us more about the mechanisms that allow it to form and then develop. Figure 10 also shows the total water vapor retrievals using SSM/T2 data for the early morning of December 21 (0200 UTC) overlaid on the nearly coincident AVHRR visible imagery. The total water vapor retrievals show that the band of cloud spiraling into the mesocyclone at around 60 °W corresponds to a tongue of moist air transported southward from the Weddell Sea. The clear slot in the visible imagery can be associated with an area of dryer air, perhaps indicating air that has descended, possibly from the high Antarctic plateau. Although the tongue of moist air is correlated with the band of cloud spiraling into the center of the mesocyclone, the rest of the cloud associated with this system does not correlate with the TWV field. This gives us more confidence that the TWV field retrieved is not seriously contaminated by clouds.

5. Conclusions

A method to retrieve the total water vapor in the atmosphere using data from the water vapor sounder SSM/T2 is developed based on both theoretical analyses and radiative transfer simulations. The method has been validated in Antarctica by comparisons with water vapor data from a numerical model and radiosondes. The high sensitivity to water vapor and the low sensitivities to ground surface and clouds (except for thick ice clouds) make this method especially useful in polar regions, where the atmospheric water vapor measurements are temporally and spatially sparse. The good coverage of DMSP satellites in polar regions enables TWV imagery over Antarctica to be obtained on a daily basis. This will benefit studies of water vapor transport and precipitation over the Antarctic ice sheet. Preliminary analyses of long-term climatology and individual weather process using retrieved TWV data show the potential of SSM/T2 for improving our understanding of the meteorology and climatology of the Antarctic.

Acknowledgments. This study was supported by the University of Bremen and partially by the European Union within the framework of COST-712 and the Deutsche Forschungsgemeinschaft under the contract code of He1746/3-1.2. SSM/T2 data are provided by NGDC, Boulder, Colorado. Comments from anonymous referees are highly appreciated.

References

Aerojet GenCorp., System summary report for the SSM/T2 water vapor profiling sensor hardware segment, Report to the Department of the Air Force, Azusa, California, 1990.

Anderson, P. S., Evidence for an Antarctic winter coastal polynya, *Antarct. Sci., 5,* 221–226, 1993.

Anderson, P. S., A method for rescaling humidity sensors at temperatures well below freezing, *J. Atmos. Oceanic Technol., 11,* 1388–1391, 1994.

Bindschadler, R., Monitoring ice sheet behavior from space, *Rev. Geophys., 36,* 79–104, 1998.

Bromwich, D. H., Snowfall in high latitudes, *Rev. Geophys., 26,* 149–168, 1988.

Bromwich, D. H., Estimates of Antarctic precipitation, *Nature, 343,* 627–628, 1990.

Burns, B. A., X. Wu, and G. R. Diak, Impact of emissivity model errors on the retrieval of water vapor profiles over ocean with SSM/T2, Paper presented at 1998 IEEE International Geoscience and Remote Sensing Symposium, Seattle, Wash., 1998.

Chang, A. T. C., P. Gloersen, and T. Schmugge, Microwave emission from snow and glacier ice, *J. Glaciol., 16,* 23–39, 1976.

Chylek, P., and V. Ramaswamy, Simple approximation for infrared emissivity of water clouds, *J. Atmos. Sci., 39,* 171–177, 1982.

Connolley, W. M., and J. C. King, Atmospheric water-vapour transport to Antarctica inferred from radiosonde data, *Q. J. R. Meteorol. Soc., 119,* 325–342, 1993.

Connolley, W. M., and J. C. King, A modeling and observation study of East Antarctic surface mass balance, *J. Geophys. Res., 101,* 1335–1343, 1996.

del Guasta, M., M. Morandi, L. Stefanutti, J. Brechet, and J. Piquad, One year of cloud data from Dumont d'Urville (Antarctica), 1, General overview of geometrical and optical properties, *J. Geophys. Res., 98,* 18,575–18,587, 1993.

Felde, G. W., and J. D. Pickle, Retrieval of 91 and 150 GHz surface emissivities, *J. Geophys. Res., 100,* 20,855–20,866, 1995.

Fuhrhop, R., T. C. Grenfell, G. Heygster, K.-P. Johnsen, P. Schlüssel, M. Schrader, and C. Simmer, A combined radiative transfer model for sea ice, open water, and atmosphere, *Radio Sci., 33,* 303–316, 1998.

Gibbins, C. J., Improved algorithms for the determination of specific attenuation at sea level by dry air and water vapor in the frequency range 1–350 GHz, *Radio Sci., 21,* 949–954, 1986.

Giovinetto, M. B., K. Yamazaki, G. Wendler, and D. H. Bromwich, Atmospheric net transport of water vapor and latent heat across 60 °S, *J. Geophys. Res., 102,* 11,171–11,179, 1997.

Grody, N. C., Remote sensing of atmospheric water content from satellites using microwave radiometry, *IEEE Trans. Antennas Propagat., 24,* 155–162, 1976.

Grody, N. C., Surface identification using satellite microwave radiometers, *IEEE Trans. Geosci. Remote Sens., 26,* 850–859, 1988.

Guissard, A., and P. Sobieski, A simplified radiative transfer equation for application in ocean microwave remote sensing, *Radio Sci., 29,* 881–894, 1994.

Hall, D. K., and J. Martinec, *Remote Sensing of Ice and Snow,* 189 pp., Chapman and Hall, New York, 1985.

Heinemann, G., Idealized simulations of the Antarctic katabatic wind system with a three-dimensional mesoscale model, *J. Geophys. Res., 102,* 13,825–13,834, 1997.

Hirasawa, N., H. Nakamura, and T. Yamanouchi, Abrupt changes in meteorological conditions observed at an inland Antarctic station in association with wintertime blocking, *Geophys. Res. Lett., 27,* 1911–1914, 2000.

Howarth, D. A., Seasonal variations in the vertically integrated water vapor transport fields over the southern hemisphere, *Mon. Weather Rev., 111,* 1259–1272, 1983.

Jacobs, S. S., H. H. Hellmer, C. S. M. Doake, A. Jenkins, and R. M. Frolich, Melting of ice shelves and the mass balance of Antarctica, *J. Glaciol., 38,* 619–637, 1992.

King, J. C., and J. Turner, *Antarctic Meteorology and Climatology,* 409 pp., Cambridge Univ. Press, Cambridge, 1997.

Kleespies, T. J., Some anomalies in the SSM/T2 antenna temperatures, Paper presented at 8th Conference on Satellite Meteorology and Oceanography, American Meteorological Society, Atlanta, Ga., 1996.

Klein, L. A., and C. T. Swift, An improved model for the dielectric constant of sea water at microwave frequencies, *IEEE Trans. Antennas Propagat., 25,* 104–111, 1977.

Köpken, C., and G. Heinemann, Assessment of the quality of TOVS retrievals obtained with the 3I algorithm for Antarctic conditions, *J. Geophys. Res., 100,* 5143–5158, 1995.

Kramer, H. L., *Observation of the Earth and Its Environment: Survey of Missions and Sensors,* 960 pp., Springer-Verlag, Berlin, 1996.

Kuo, C. C., D. H. Staelin, and P. W. Rosenkranz, Statistical iterative scheme for estimating atmospheric relative humidity profiles, *IEEE Trans. Geosci. Remote Sens., 32,* 254–260, 1994.

Laue, H., Bestimmung von antarktischen Bodenemissivitäten mit Hilfe von Radiosonden- und Satellitendaten, Master Thesis, 98 pp., Inst. of Environ. Phys., Univ. of Bremen, Bremen, Germany, 1999.

Loewe, F., The transport of snow on ice sheets by the wind, in Studies on Drifting Snow, Publ. 13, pp. 1–69, Dep. of Meteorol., Univ. of Melbourne, Melbourne, Victoria, Aust., 1970.

Miao, J., Retrieval of atmospheric water vapor content in polar regions using spaceborne microwave radiometry, *Rep. Polar Res. 289/98,* 109 pp., Alfred Wegener Inst. for Polar and Mar. Res., Bremerhaven, Germany, 1998.

Oerlemans, J., Effect of irregular fluctuations in Antarctic precipitation on global sea level, *Nature, 290,* 770–772, 1981.

Schlüssel, P., and W. J. Emery, Atmospheric water vapor over oceans from SSM/I measurements, *Int. J. Remote Sens., 11,* 753–766, 1990.

Staelin, D. H., K. F. Kunzi, R. L. Pettyjohn, K. L. Poon, R. W. Wilcox, and J. W. Waters, Remote sensing of atmospheric water vapor and liquid water with the Nimbus 5 microwave spektrometer, *J. Appl. Meteorol., 15,* 1204–1214, 1976.

Stone, R. S., Properties of austral winter clouds derived from radiometric profiles at the South Pole, *J. Geophys. Res., 98,* 12,961–12,971, 1993.

Susskind, J., J. Rosenfield, and D. Reuter, Remote sensing of weather and climate parameters from HIRS2/MSU on TIROS-N, *J. Geophys. Res., 89,* 4677–4697, 1984.

Turner, J., T. A. Lachlan-Cope, J. P. Thomas, and S. R. Colwell, The synoptic origins of precipitation over the Antarctic Peninsula, *Antarct. Sci., 7,* 327–337, 1995.

Turner, J., S. R. Colwell, and S. Harangozo, Variability of precipitation over the coastal western Antarctic Peninsula from synoptic observations, *J. Geophys. Res., 102,* 13,999–14,007, 1997.

Ulaby, F. T., R. K. Moore, and A. K. Fung, *Microwave Remote Sensing: Active and Passive,* 2162 pp., Artech House, Norwood, Mass., 1981.

Wilheit, T. T., and K. D. Hutchison, Water vapor profile retrievals from SSM/T2 data constrained by infrared-based cloud parameters, *Int. J. Remote Sens., 18,* 3263–3277, 1997.

Zwally, H. J., Microwave emissivity and accumulation rate of polar firn, *J. Glaciol., 18,* 195–215, 1977.

Zwally, H. J., Growth of Greenland ice sheet: Interpretation, *Science, 246,* 1589–1591, 1989.

G. Heygster, K. Kunzi, and J. Miao, Institute of Environmental Physics, University of Bremen, 28334 Bremen, Germany. (jungang.miao@physik.uni-bremen.de)

T. A. Lachlan-Cope and J. Turner, British Antarctic Survey, Madingley Road, Cambridge, CB3 0ET, England, United Kingdom. (tlc@pcmail.nerc-bas.ac.uk)

(Received March 28, 2000; revised November 13, 2000; accepted November 14, 2000.)